Spectral analysis combined with nonlinear optical measurement of laser printed biopolymer composites comprising chitosan/SWCNT

Mikhail S. Savelyev[a,b,∗], Alexander Yu. Gerasimenko[a,b], Pavel N. Vasilevsky[a], Yulia O. Fedorova[a], Thomas Groth[b,c], Galina N. Ten[d], Dmitry V. Telyshev[a,b]

[a] Institute of Biomedical Systems, National Research University of Electronic Technology, 124498, Zelenograd, Moscow, Russian Federation
[b] Institute for Bionic Technologies and Engineering, I.M. Sechenov First Moscow State Medical University, 119991, Moscow, Russian Federation
[c] Department Biomedical Materials, Institute of Pharmacy, Martin Luther University Halle-Wittenberg, 06120, Halle, Saale, Germany
[d] Department of Radiotechnology and Electrodynamics, Saratov State University, 410012, Saratov, Russian Federation

A B S T R A C T

Biopolymer composites based on two types of chitosan (chitosan succinate and low-molecular weight chitosan) with single-walled carbon nanotubes (SWCNT) were created by laser printing. SWCNT have good dispersibility in chitosan solutions and therefore, can form relatively homogeneous films that was shown in scanning electron microscopy images. For the studies film composites were formed under the action of laser radiation on aqueous dispersion media. Study of the nonlinear optical process during the interaction of laser radiation with a disperse media has shown that low-molecular chitosan has a large nonlinear absorption coefficient of 17 cm/GW, while the addition of SWCNT lead to a significant increase up to 902 cm/GW. The threshold intensity for these samples was 5.5 MW/cm^2 with nanotubes. If intensity exceeds the threshold value, nonlinear effects occur, which, in turn, lead to the transformation of a liquid into a solid phase. Characterization of films by FTIR and Raman spectroscopy indicated arising molecular interactions between chitosan and SWCNT detected as a small frequency shift and a change in the shape of radial breathing mode (RBM). The results indicate the possibility using aqueous dispersion media based on chitosan and SWCNT to create three-dimensional films and scaffolds for tissue engineering by laser printing.

1. Introduction

Cardiac surgery is very important for the maintenance of human life and health in most modern societies [1]. First of all, it is necessary to create means capable of ensuring rapid hemostasis and repair in case of pathological changes of blood vessels and cardiac tissue [2]. Implantable devices with biocompatible coatings like stents, artificial heart valves, ventricular assists devices are used to restore the hemodynamic function of the hearth [3]. On the other hand, repair of cardiac tissue has been addressed for some time by the development of technologies using tissue engineering that is based on combination of some scaffold material with living cells [4]. In this regard, the direction of creating three-dimensional structures targeted to improve the recovery of damaged tissues of the heart and blood vessels begin to develop [5]. Nowadays, scaffold scan be also fabricated by 3D printing methods, colonized by cells and serve then as a replacement tissue during the recovery process [6]. One of the most effective methods for creating tissue-engineering scaffolds is laser printing, as it allows to form

scaffolds with complex structure with high accuracy [7].

One of the laser printing methods, allowing the formation of porous structures for subsequent cell colonization, is selective laser sintering. This method is based on layer-by-layer sintering of fine powder in accordance with a predetermined 3D model. In previous work, the possibility of using selective laser sintering to create scaffolds for cardiac tissue engineering was shown [8]. A scaffold made of polycaprolactone powder was obtained with support of pulsed laser radiation with a power of 3 W and a pulse repetition rate of 150 Hz. The resulting scaffold had a high porosity of > 80% with at the pore size 40–100 μm. It was shown that cells were adhering on this material, which led to the formation of a stable cell colony over time [8]. To create tissue-engineering structures of a hemispherical geometry, the method of dynamic optical projection stereolithography was applied in another study [9]. A polyethylene glycol diacrylate prepolymer solution was used as a printing material. In this technology, the scanning system of mirrors allows to polymerize liquids at several points of one layer at once, which significantly increases the speed of three-dimensional

---

structures printing. Using confocal microscopy, it was found that the resulting scaffolds provided good adhesion and proliferation of fibroblasts [9]. Moreover, the best formation of the tissue structures from fibroblast was observed when the size of pores was in the range of 160 μm. The disadvantage of this system is the use of laser with a wavelength in the UV range as laser radiation source, which can damage the polymer structure and cells [10]. Material formation through layer-by-layer deposition is promising for prepare nanocoatings on arteries [11].

Another promising technology for creating tissue-engineering scaffolds is the method of composite formation by laser radiation in visible and infrared wavelength range of light. We have shown previously that biopolymers like albumin, collagen and single-walled carbon nanotubes can be used as materials for the formation of biocompatible nanocomposites by this method [12]. Carbon nanotubes with low concentrations in total mass of the material, which are able to impart electrical conductivity and improve mechanical properties, such as hardness and tensile strength [13], is used in this method. Thus, it is possible to create electrical conductive and biocompatible tissue-engineering structures to be used for the heart tissue restoration by laser printing methods based on synthetic materials [14]. The use of synthetic polymers like polycaprolactone, acrylate polymers, etc. has a number of disadvantages, such as low bioresorbability and weak mechanical characteristics. As a result, the search for new materials that would provide the best characteristics for tissue engineering of the cardiovascular system continues.

To create structures and coatings for implantable devices, materials based on the biopolymer chitosan are often used due to the abundance of this material and its good biocompatibility [15]. In a previous study, an electrospinning method was used to obtain fiber scaffolds based on blends of chitosan and poly (lactic acid). Scaffolds, made of this polymer blend nanofibers, showed good mechanical characteristics, as well as ensured high viability of cardiomyocytes and increased the secretion of troponin involved in the process of cardiac muscle contraction [16]. Three-dimensional structures can be also obtained by electrophoretic deposition of biocompatible materials on substrates [17]. A given pattern was formed on the surface of the titanium substrate by laser ablation. Nd: YVO$_4$ solid-state laser with a wavelength of 532 nm, a power of 8 W, a radiation frequency of 200 kHz and a pulse duration of 12 ns was used for ablation. Then, layers of chitosan and collagen were subsequently deposited onto the substrate. The resulting scaffolds supported the proliferation and adhesion of myoblasts and fibroblasts. In addition, it was possible to use chitosan-based hydrogels for the restoration of cardiac tissue [18]. To create such three-dimensional scaffolds, it is also proposed to use a chitosan matrix filled with functional nanoparticles [19]. For example, a hydrogel was prepared from a 2% solution of chitosan, which was mixed with an aqueous dispersion of gold nanoparticles. The nanoparticles provided the hydrogel with electromechanical properties comparable to the characteristics of the heart tissue. Such a hydrogel ensured high viability and growth rate of mesenchymal stem cells [18]. Another option is the use of carbon nanotubes as such filler for the matrix, because they contribute to the improvement of the electrical conductive and mechanical characteristics of the structure [20]. In addition, such material will have a good biodegradability and will be completely removed from the site of defect in the cardiovascular tissues after healing [21].

The paper presents the results of spectral and nonlinear optical studies of dispersed media based on chitosan mixed with single-wall carbon nanotubes. In this paper, studies have been carried out to use laser radiation in the visible range of spectrum to form biopolymer composites based on chitosan and carbon nanotubes, since the use of ultraviolet radiation, which is strongly absorbed by chitosan [22,23] increases the risk of destruction of encapsulated cells [10]. The determination of these characteristics is important for fabricating three-dimensional structures based on biopolymers with desired architecture by 3D laser printing methods. Knowing the interaction of laser radiation with materials like polymers and fillers, parameters can be varied for

the formation of scaffolds with different structures, which is important for cardiac tissue engineering. Chitosan-based media are well suited for fabricating scaffolds with desired shape and interconnected porosity [24]. Adding carbon nanotubes to the dispersion can improve the mechanical and electrical characteristics of the created scaffold [25]. Such dispersions can be used as ink for creation of films and scaffolds for tissue engineering by laser radiation that can later be used in cardiovascular surgery.

2. Materials and experimental details

2.1. Materials

Low-molecular chitosan (LMC) («Bioprogress», Moscow, Russia) produced by chemical hydrolysis from a high-molecular-weight chitosan was delivered as powder [26]. Chitosan succinate (CS) was formed by the reaction of succinic acid with chitosan according to the information obtained from the producer («Bioprogress», Moscow, Russia). Both types of chitosan used in this work are water soluble, since their molecular weight is below 50 kDa. Distilled water was used as a solvent (pH - 5.8–6.1). To obtain a homogeneous aqueous dispersed medium, aqueous paste of carbon nanotubes with a concentration of 2.6% (w/w) was used (Carbon Chg Ltd., Chernogolovka, Russia).

2.2. Fabrication of dispersions of carbon nanotubes with chitosan

The preparation process of aqueous dispersed media took place in two stages. The first stage included mixing distilled water with nanotube paste to obtain a concentration of 0.001% (w/w). An ultrasonic homogenizer Sonicator Q700 (Qsonica, Newtown, U.S.) was used for 1 h at a power of 40 W, followed by further mixing on a magnetic stirrer for 30 min. Then, chitosan (either LMC or CS) was stepwise added as powder to the aqueous dispersion of carbon nanotubes under constant stirring until a concentration of 2% (w/w) was reached. The final dispersion, similarly to the previous step, was subjected to ultrasound (with a smaller power in the ultrasonic bath) for 90 min and then stirred with a magnetic stirrer for another 20 min. Fig. 1 shows a typical view of prepared dispersions in cuvettes with an optical path length of 2 mm.

The absorption spectra of chitosans and their aqueous dispersions with SWCNT were measured to monitor the stability of samples against sedimentation. The absorption spectra were measured in the range of 250–1100 nm with a resolution of 1 nm. A Genesis UV–Vis instrument (Thermo Fisher Scientific™, Waltham, U.S.) was used for the measurements. A cuvette with an optical path length of 2 mm was fixed in a
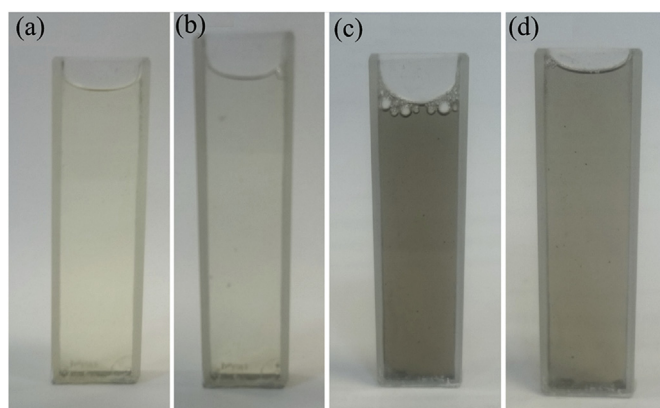

Fig. 1. Aqueous dispersions of carbon nanotubes with chitosan in cuvettes: (a) – Chitosan succinate 2% (w/w), (b) – Low-molecular chitosan 2% (w/w), (c) – Chitosan succinate 2% (w/w) + SWCNT 0.001% (w/w), (d) – Low-molecular chitosan 2% (w/w) + SWCNT 0.001% (w/w).
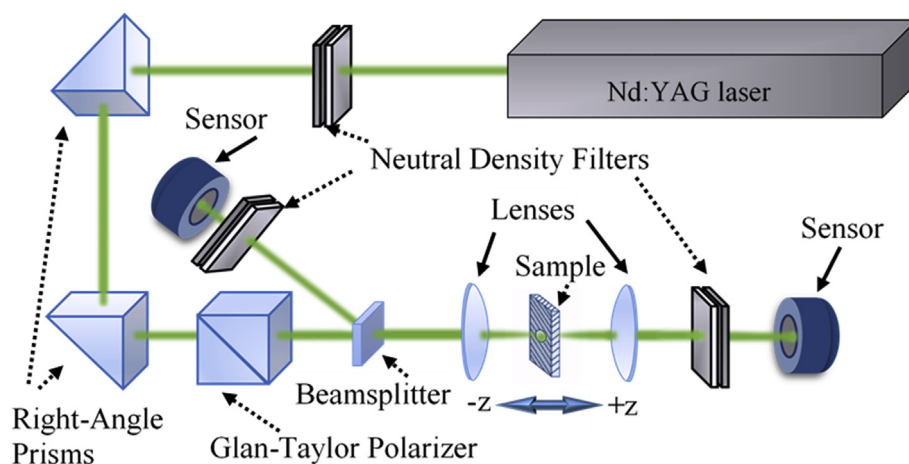
Fig. 2. The scheme for investigation of samples nonlinear optical properties.
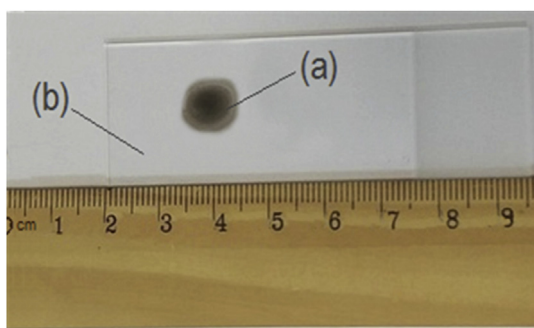

Fig. 3. Laser dried film sample prepared for spectral measurements: (a) – film, (b) – glass slide.

special holder that allows working with different optical path lengths from 1 mm to 5 mm.

2.3. Measurement of nonlinear optical data

For a better understanding of the nature of laser radiation interaction, studies of nonlinear characteristics of aqueous solutions/dispersions of chitosan (both types) with and without SWCNT were carried out. The clarified parameters will form the basis of the laser printing process. The experimental set-up is shown in Fig. 2. It includes a nanosecond solid-state Nd:YAG laser with pulse duration of ~16 ns as the radiation source. To collect data about the samples, its second harmonic of radiation with a wavelength of 532 nm and linear polarization was used. A control of the pulse energy was implemented using a set of neutral density filters. The right-angle prisms were used to rotate the beam around 180°. Later, the beam hits the Glan-Taylor polarizer. A fine adjustment of the linearly polarized pulse energy was achieved by rotating the prism in a plane that was perpendicular to the direction of radiation propagation. The plate beamsplitter, neutral density filters and the Ophir PD-10 sensor are used to monitor the pulse energy incident on the sample. Flat convex lenses are fixed confocal, their focal lengths are the same and equal to 10 cm. The sample is fixed in a holder on a motorized ruler. The value of the pulse energy transmitted through the sample is determined by the Ophir PE-9 sensor. The neutral density filters are used to avoid a possible damage of sensor. The energy of laser radiation U, depending on the position of the sample z, is related to the intensity I by the ratio:

$$U(z) = \int\limits_{-\infty}^{+\infty} \int\limits_{0}^{2\pi} \int\limits_{0}^{\infty} I(\rho, \phi, z, t, d)\rho d\rho d\phi dt.$$

(1)

where ρ and ϕ are the polar coordinates in the cross section of the laser beam, t is the time in the temporal pulse shape, and d is the thickness of the sample.

The installation allows collecting data to study the nonlinear optical properties by two methods. The first one is an open-aperture Z-scan [27]. At a constant pulse energy, the sample was moved relative to the lens focus along the direction of beam propagation. It was possible to transfer the sample to the side, to prevent the heat accumulation effect in the local area from the pulses passage, since the temperature of the irradiated area strongly affects the nonlinear optical characteristics [28]. The second one is a fixed sample location method [29]. Adjusting the incident pulse energy is achieved using light filters and Glan-Taylor polarizer, while the size of the laser spot on the sample remains unchanged.

2.4. Spectral measurement of the materials used

Before measuring the infrared and Raman spectra, film samples were prepared (Fig. 3). Aqueous dispersions were spotted on a glass slide and dried by laser irradiation. To do this, the unfocused laser beam was directed to the dispersion droplets on the substrate from top to bottom. As source of laser radiation a Titanium-Sapphire femtosecond laser (Ti:Sa), operated at 810 nm wavelength with pulse duration of 140 fs and frequency 80 MHz, was used [12]. The radiation affected one area of dispersion until the water evaporated at a temperature of around 40–50 °C. Additionally, samples of the pure components of dispersions: LMC, CS and a dehydrated paste of SWCNT were prepared as a basis for comparison.

The absorption spectra of samples in the IR range were used to determine the difference in the properties of chitosan depending on the degree of deacetylation and chemical modification. This indicator allows the evaluation of biological properties [30] and water solubility [15,31] (water-holding and fat-retaining properties). Since the process of deacetylation of chitosan comprises the removal of acetyl groups from the molecular chain of a polymer, this leads to an increase in its hydrophobicity [32]. The spectra were measured in the infrared range of 4000–400 cm^{-1} by the attenuation total reflectance method using a Nicolet iS50 Fourier spectrometer (Thermo). Raman spectra were measured to determine the characteristics of SWCNT in the composite by analysing the D, G and RBM band [33]. The LabRAM HR Evolution (Horiba) spectrometry complex equipped with a HeNe laser with a wavelength of 633 nm, operating range for registering the Raman shift of 100–1800 cm^{-1}.
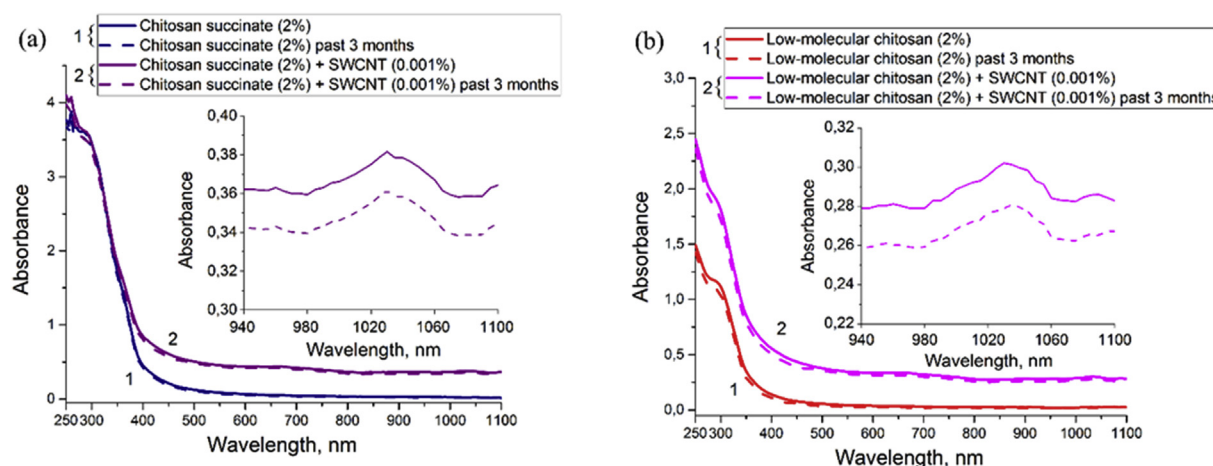
Fig. 4. The UV–Vis absorption spectra of aqueous dispersions: (a) – Chitosan succinate (2%), (b) – Low-molecular chitosan (2%).

2.5. Scanning electron microscopy

To evaluate the structure of the formed biopolymer composites, film samples on a silicon substrate were formed and studied by scanning electron microscopy (SEM). For this, a FEI Helios NanoLab 650 scanning electron microscope with accelerating voltage of 2 kV, electron probe current 0,17 nA was used.

3. Results

3.1. Characterization of linear and nonlinear optical properties

Fig. 4 presents the absorption spectra of dispersions by UV/Vis spectrometry in the range from 250 to 1100 nm. The spectra show that both types of chitosan possess a strong peak of absorption in the UV range, while dispersions with SWCNT have additional weak absorption peaks in the near-infrared range. Fig. 4 clearly shows the difference in the peak of absorbance in the wavelength range of 250–350 nm between CS and LMC. The difference in optical density in the ultraviolet range between the two types can be associated with different methods for producing chitosan.

In addition, the spectra were used to control absorbance for monitoring the stability of samples against sedimentation. It was established that during the observation period of 3 months no sedimentation of dispersion components was observed, which was confirmed by the optical spectrum in the range of 250–1100 nm, which did not change. The obtained spectra show a strong influence of chitosan type on the optical properties, especially in UV range.

Next, measurements of non-linear optical properties of samples were carried out with the laser equipment. First, the value of the linear absorption coefficient was determined in accordance with Beer-Lambert's law in experiments with low intensity of radiation input, when nonlinear effects are not yet manifested. Fig. 5a shows the dependencies of the normalized transmission on the sample position. Normalizing was carried out relatively to the transmission values in the linear mode. The radius of the laser beam at the focus was 23 μm. A CCD-camera was used for this purpose.

The optical characteristics were calculated based on the radiation transfer equation [34]:

$$\int_{I_0(\rho,z,t,0)}^{I(\rho,z,t,d)} \frac{1}{I\mu(I)} dI = -\int_0^d dl,$$

(2)

where l is the coordinate along the direction of beam propagation inside the sample, $\mu(I)$ is the absorption coefficient which, in the "threshold" model can be set by a function whose graph is shown in the logarithmic scale on Fig. 6. For such a dependence of the absorption coefficient on

the intensity, one can obtain the solution of equation (2) explicitly describing the change in the transmitted intensity from the incident one. The support of the obtained expression in (1) allows us to determine the energy of a single laser pulse and the normalized transmission in the final stage. Using the threshold dependence of the total absorption coefficient on the intensity for calculation of nonlinear optical parameters was described in our article published recently [35]. The advantage of using such model is the ability to describe nonlinear attenuation in the case of the synergistic effect of absorption and scattering inherent in disperse media.

Fig. 6 shows the dependence of the absorption coefficient in the presence of the threshold effect. The model itself does not take scattering into account, however, in the case of the synergistic action of these effects, it allows to describe the Z-scan and fixed sample location experiments more accurate [35]. In the case of studying dispersed media, the limiting threshold value can be related to the critical radius of microbubbles, upon reaching which a noticeable contribution to the attenuation of laser radiation begins and, as a result, an insufficiently accurate description of this process by the non-threshold model [29].

The addition of SWCNT to chitosan-water dispersion leads to an increase in the linear and nonlinear absorption coefficient, which characterizes the passage of laser radiation through the sample (Table 1). However, an increase in energy leads to a sharp decrease in the transmitted single pulse energy due to the manifestation of nonlinear effects from SWCNT. Moreover, nonlinear effects occur at lower radiation intensity. Pure chitosan exhibited weak nonlinear effects; transmission of samples began to decrease only near the lens focus (at a distance of 2 cm from the lens, with z equal to −2 and 2 cm as shown in Fig. 5). When carbon nanotubes were added, dispersions showed significantly stronger non-linear effects (normalized transmittance at point z = 0 cm). At the same time, the normalized transmission also approaches to 1, however, more slowly (more distance from the lens focus) than in dispersions without SWCNT. Thus, the manifestation of nonlinear effects in dispersion SWCNT with chitosan requires significantly lower values of the incident radiation intensity (Table 1).

3.2. Spectral analysis of chitosan/SWCNT solutions and composite films

The properties of the carbon nanotubes structure are clearly seen in the Raman spectra (data for pure samples of dehydrated paste are presented separately in Fig. 7a). As it can be seen from the graphs, all of the characteristic carbon nanotube bands are presented: the RBM (about 150–250 cm^{-1}), represented by a narrow band with different peaks, which indicates the presence of tubes with different diameters; mode D (about 1300 cm^{-1}) which in comparison with the intensity of the G mode (about 1600 cm^{-1}) characterizes the low defectiveness of
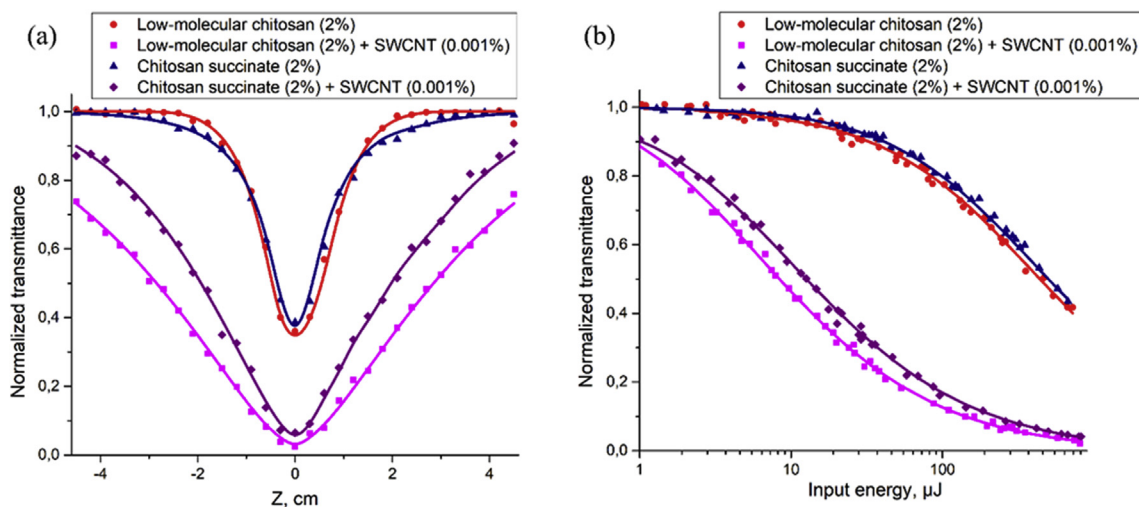
Fig. 5. Dependence of normalized transmission: (a) – on the position of LMC, LMC + SWCNT, CS, CS + SWCNT samples relative to the lens; (b) – on the incident beam energy of samples based on LMC, LMC + SWCNT, CS, CS + SWCNT. Lines show theoretical curves.

the tube structure. It was also found that carbon nanotubes exhibit semiconductor properties (this is characteristically manifested as the location of G^- and G^+ modes of the G band) [36,37]. Partial coincidence of frequencies for the peaks corresponding to the nanotube modes and the Amide bands (in the region of 1300 cm^{-1}, 1600 cm^{-1}) complicates the analysis of the obtained results. However, the presence of RBM and distinctive G peak for both samples indicate the stability of the nanotubes against laser radiation.

As it can be seen from the FTIR spectra (Fig. 7b), Amide bands characteristic for organic chitosan appeared as peaks around 1630, 1540 and 1320 cm^{-1} (Amide I, II and III respectively). A broad peak in the region of 3000–3500 cm^{-1} is indicative for the presence of N–H groups (Amide A, B). The difference in the form of peaks in this spectral range for two types of chitosan indicated a different chemical composition. The change in the intensity and ratio of amide bands for two types of chitosan on the FTIR spectrum provided evidence that the degree of deacetylation of chitosan succinate is higher, which results in its greater degree of hydrophobicity. Also, chitosan succinate sample films exhibited lesser brittleness compared to the other type. Also, a difference in the intensity of the bands for sample of chitosan with carbon nanotubes compared to a pure sample without SWCNT was noticed since nanotubes greatly absorb in IR range [38–40].

Studies show that chitosan showed stability against to laser radiation – FTIR spectra represent the Amide bands for both samples after laser radiation that confirmed the stability of the chitosan to this kind of exposure [41,42].

3.3. Characterization of films by scanning electron microscopy

As it can be seen in Fig. 8, the surface of the film with low-molecular chitosan is much flatter and more homogeneous, while convex rounded structures are visible on the film surface with chitosan succinate, which shows the effect of the chemical composition of chitosan on sample uniformity. The images also show a uniform distribution of carbon nanotubes over the entire surface of the film. Also randomly directed conglomerates of SWCNT are found on the surface, which demonstrates the stability of them under the action of laser radiation.

4. Discussion

Both types of chitosan strongly absorbed radiation in the UV range according to the spectra even at very low energy values (shown in Fig. 4), which indicates the high probability of damage inflicted on the structure when using laser radiation of a wavelength below 350 nm for the formation of three-dimensional composites. The transmission of LMC and SWCNT aqueous dispersions was lower than that of CS and SWNCT dispersions with the same concentration of each chitosan (2% (w/w)). It can be assumed that this effect can be explained by the different degree of agglomeration of the nanotubes after addition to the solutions. Moreover, the normalized transmission has a smaller value in
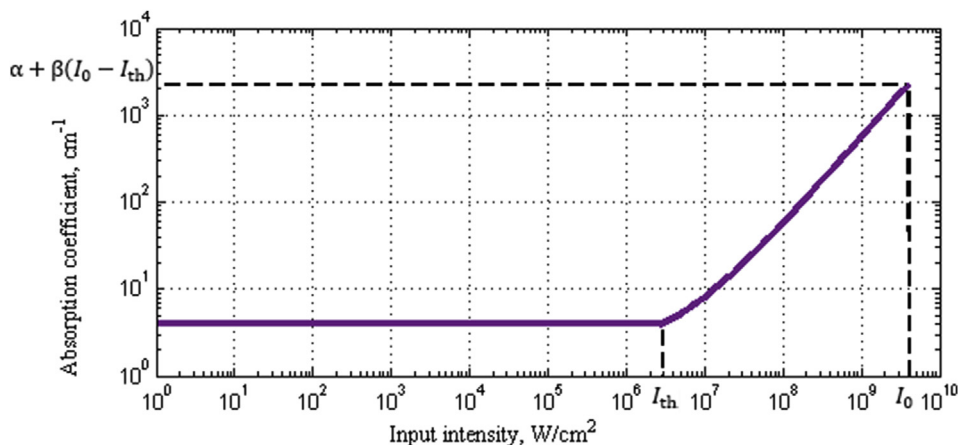

Fig. 6. Dependence of absorption coefficient on the radiation intensity. For these calculations, we used the parameters corresponding to the sample CS + SWCNT.

Table 1
Linear and nonlinear optical coefficient values.

Sample	Intensity in the beam waist «I_0» (GW/cm^2)	Linear absorption coefficient «α» (cm^{-1})	Nonlinear absorption coefficient «β» (cm/GW)	Threshold intensity « I_{th}» (MW/cm^2)
LMC (2%)	4.5	2.2	17	7.5
LMC (2%) +SWCNT (0.001%)	4.1	2.8	902	5.5
CS (2%)	5.1	2.9	16	39.0
CS (2%) + SWCNT (0.001%)	4.9	3.9	561	2.7

the case of LMC and SWCNT dispersion, which also indicates a better mixing of carbon nanotubes leading to a smaller agglomerate size [43].

It can be seen that dispersions with SWCNT sharply reduce the transmission of light with increasing input energy (Fig. 5b). Water dispersions with SWCNT absorb much more laser radiation than dispersions without SWCNT in accordance to the values of the nonlinear absorption coefficients, which was calculated from the experimental results. This effect can be explained by an increase in the optical path of the laser radiation inside the sample due to the increase in scattering that is characteristic for nanotubes. Thus, it can be concluded that an increase in the scattering of radiation leads to an increase in absorption. The results from other investigations already demonstrated that the presence of nanotubes can lead to both of these effects [44]. Thus, the study of the nonlinear optical process in the interaction of laser radiation with a disperse medium showed that the nonlinear absorption coefficient of LMC with SWCNTs increased from 17 cm/GW to 902 cm/GW. The threshold intensity, which means a transition from a linear to a nonlinear process of interaction of laser radiation with dispersed media based on SWCNTs for LMC, was 5.5 MW/cm^2. The nonlinear

absorption coefficient for CS with SWCNTs was noticeably lower (561 cm/GW), which can be explained by the large size of the formed agglomerates and correspondingly, the smaller number of fractions in the dispersion [45]. However, the limiting threshold was lower, which is associated with a weaker effect of van der Waals forces. In addition, the presence of anionic groups in CS as well as in SWCNT leads to a weaker interaction of CS and carbon nanotubes because of Coulomb repulsive force. Thus, nanotubes transfer their heat to the liquid directly [46]. CS does not decrease the formation of bubbles, which contributes to the general attenuation of radiation by increasing scattering along with absorption [47].

The main difference in the structure of the two types of chitosan used (due to their chemical composition and properties as consequence) was visible by differences of the amide bands (1630, 1540 cm^{-1}) on the FTIR spectrum. According to the data in Fig. 8b, it is clearly seen that the peak of carbonyl groups of SWCNT at ~1720 cm^{-1} becomes weaker, the N–H deformation of LMC at 1562 cm^{-1} shifts to 1513 cm^{-1} and their intensities become relatively strong. This could be related to an electrostatic attraction between cationic groups in LM and
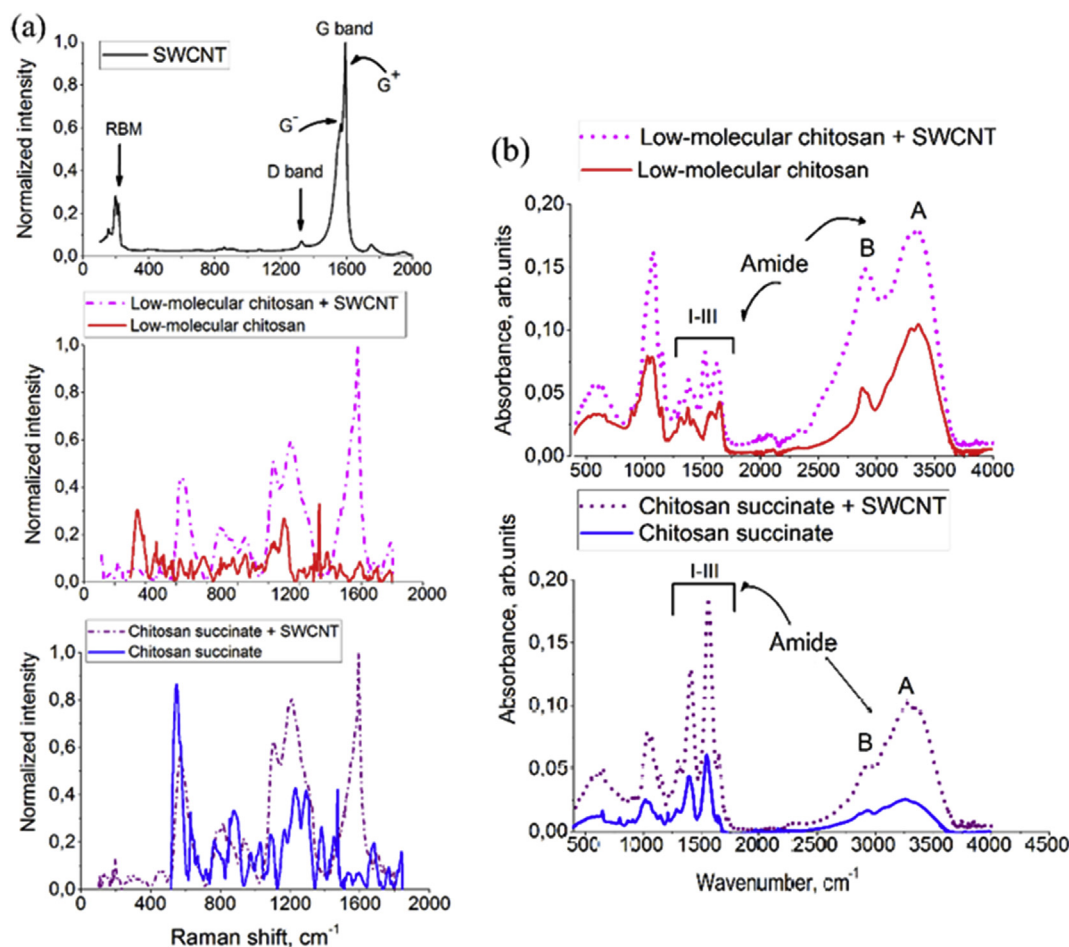

Fig. 7. Film samples based on LMC and CS with SWCNT: (a) – Raman spectra; (b) – FTIR spectra.
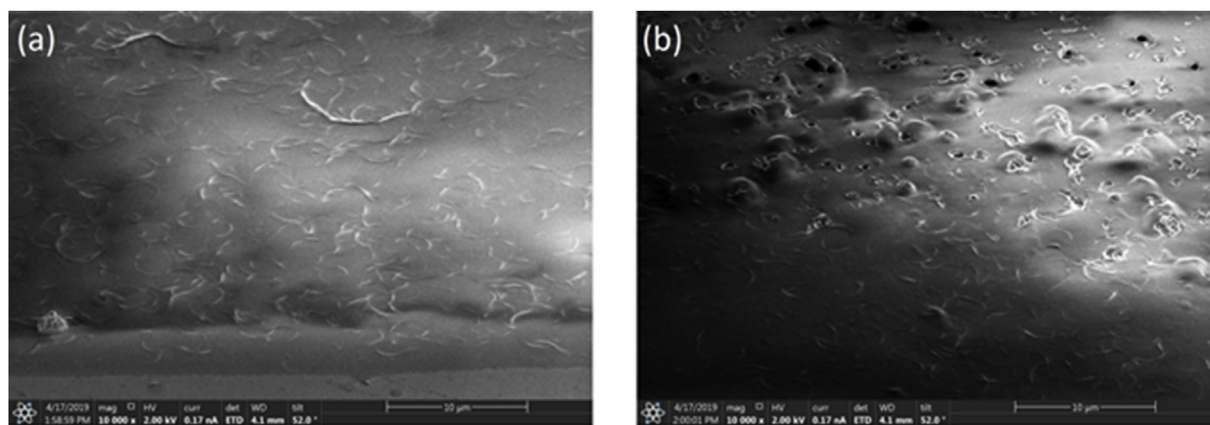
Fig. 8. SEM images of film samples: (a) – LMC with SWCNT, (b) – CS with SWCNT.

carboxyl groups of SWCNT. A similar effect of binding of chitosan to MWCNTs using ionic liquids was observed in a previous study [48]. According to the FTIR spectrum of CS + SWCNT, peak displacements were not detected; only their amplification occurred. In CS, the anionic nature of the succinic acid leads to some electrostatic repulsion between CS and negatively surface charged SWCNT.

This was also indicated by differences in intensities of the Raman spectra. The slight frequency shift in the spectra for the LMC + SWCNT and change of RBM shape are supposed to be associated with the manifestation of connections with nanotubes: under the action of laser radiation, chitosan chains interact with the surface of nanotubes, which allows the formation of a stable homogeneous biopolymer matrix. Also, the addition of carbon nanotubes can reduce the energy of the used laser radiation by increasing the absorption, which will reduce the possible detriment to organic components in the biopolymer composites aimed for medical applications.

It is known that the use of carbon nanotubes in aqueous dispersions of biopolymers, such as proteins or amino sugars, improves the stability of CNTs and increases the biocompatibility of such composite materials [49]. It is interesting to note that the embedding of carbon nanotubes in a biopolymer matrix increases their hemocompatibility and reduces the activity for platelet formation [11] due to the fact that polymers like chitosan wraps around carbon nanotubes [50]. In addition to the good electrical conductivity and mechanical characteristics of chitosan/carbon films and composites, the good blood compatibility make such materials interesting for cardiac tissue engineering.

5. Conclusion

Biopolymer composites based on aqueous dispersions of pure chitosan with carbon nanotubes were prepared using the method of evaporation by laser radiation on a glass substrate at a temperature around 40–50 °C. FTIR and Raman spectroscopy results showed that weak molecular interactions arise between chitosan and carbon nanotubes, which leads to the formation of a biopolymer matrix, as it was proved by scanning electron microscopy. The difference in the chitosan chemistry resulted in different non-linear optical properties and morphology of film samples. Nonlinear optical coefficients of liquid dispersions were calculated based on Z-scan and fixed sample location experiments. Dispersions with SWCNT showed nonlinear absorption coefficient values 50 times greater than solutions without SWCNT. It was also found that these samples have reduced threshold radiation intensity at which nonlinear optical effects begin to appear. They, in turn, lead to an increase in the absorption of laser radiation and the formation of voxels in the solid phase. It was also shown that LMC is more suitable for the formation of films by laser radiation, because of a stronger interaction of this kind of chitosan with SWCNT. The parameters of the preparation of dispersed media and laser irradiation

obtained here can form the basis of a laser printing process of biopolymer composites that is useful for the making of three-dimensional tissue engineering structures as well as for coating implantable devices that are used to treat diseases of the cardiovascular system and other tissues and organs.

Author contributions - CrediT

Mikhail S. Savelyev – Writing – original draft, Formal analysis.
Alexander Yu. Gerasimenko – Conceptualization, Writing – review & editing, Supervision, Validation.
Pavel N. Vasilevsky – Writing – original draft, Investigation.
Yulia O. Fedorova – Writing – original draft, Investigation.
Thomas Groth – Writing – review & editing.
Galina N. Ten – Conceptualization.
Dmitry V. Telyshev – Project administration, Validation.

Declaration of competing interest

The authors declare that they have no known competing financial interests or personal relationships that could have appeared to influence the work reported in this paper.

Acknowledgements

References

[1] C. Lawrence, A. David, Cardiac Surgery in the Adult, fifth ed., McGraw-Hill Education - Europe, New York, United States, 2017.

[2] M. Owens, A. Senrud, J. Teach, K. Gregory, A device for the deployment of internal esophageal chitosan bandage, Gastrointest. Endosc. 63 (2006) AB237, https://doi.org/10.1016/j.gie.2006.03.612.

[3] S.H. Lee, N. Doliba, M. Osbakken, M. Oz, D. Mancini, Improvement of myocardial mitochondrial function after hemodynamic support with left ventricular assist devices in patients with heart failure, J. Thorac. Cardiovasc. Surg. 116 (1998) 344–349, https://doi.org/10.1016/S0022-5223(98)70136-9.

[4] R. Gaetani, P.A. Doevendans, C.H.G. Metz, J. Alblas, E. Messina, A. Giacomello, J.P.G. Sluijter, Cardiac tissue engineering using tissue printing technology and human cardiac progenitor cells, Biomaterials 33 (2012) 1782–1790, https://doi.org/10.1016/j.biomaterials.2011.11.003.

[5] R.K. Kankala, K. Zhu, J. Li, C.-S. Wang, S.-B. Wang, A.-Z. Chen, Fabrication of arbitrary 3D components in cardiac surgery: from macro-, micro- to nanoscale, Biofabrication 9 (2017) 032002, , https://doi.org/10.1088/1758-5090/aa8113.

[6] A.-V. Do, B. Khorsand, S.M. Geary, A.K. Salem, 3D printing of scaffolds for tissue regeneration applications, Adv. Healthc. Mater. 4 (2015) 1742–1762, https://doi.org/10.1002/adhm.201500168.

[7] A. Accardo, M.-C. Blatché, R. Courson, I. Loubinoux, C. Thibault, L. Malaquin, C. Vieu, Multiphoton direct laser writing and 3D imaging of polymeric freestanding

architectures for cell colonization, Small 13 (2017) 1700621, , https://doi.org/10.1002/smll.201700621.

[8] W.Y. Yeong, N. Sudarmadji, H.Y. Yu, C.K. Chua, K.F. Leong, S.S. Venkatraman, Y.C.F. Boey, L.P. Tan, Porous polycaprolactone scaffold for cardiac tissue engineering fabricated by selective laser sintering, Acta Biomater. 6 (2010) 2028–2034, https://doi.org/10.1016/j.actbio.2009.12.033.

[9] A.P. Zhang, X. Qu, P. Soman, K.C. Hribar, J.W. Lee, S. Chen, S. He, Rapid fabrication of complex 3D extracellular microenvironments by dynamic optical projection stereolithography, Adv. Mater. 24 (2012) 4266–4270, https://doi.org/10.1002/adma.201202024.

[10] L. Elomaa, C.-C. Pan, Y. Shanjani, A. Malkovskiy, J.V. Seppälä, Y. Yang, Three-dimensional fabrication of cell-laden biodegradable poly(ethylene glycol-co-depsipeptide) hydrogels by visible light stereolithography, J. Mater. Chem. B. 3 (2015) 8348–8358, https://doi.org/10.1039/C5TB01468A.

[11] T. Groth, A. Lendlein, Layer-by-Layer deposition of polyelectrolytes—a versatile tool for the in vivo repair of blood vessels, Angew. Chem. Int. Ed. 43 (2004) 926–928, https://doi.org/10.1002/anie.200301708.

[12] A.Y. Gerasimenko, O.E. Glukhova, G.V. Savostyanov, V.M. Podgaetsky, Laser structuring of carbon nanotubes in the albumin matrix for the creation of composite biostructures, J. Biomed. Optic. 22 (2017) 065003, , https://doi.org/10.1117/1.JBO.22.6.065003.

[13] A.Y. Gerasimenko, A.A. Dedkova, L.P. Ichkitidze, V.M. Podgaetskii, S.V. Selishchev, A study of preparation techniques and properties of bulk nanocomposites based on aqueous albumin dispersion, Optic Spectrosc. 115 (2013) 283–289, https://doi.org/10.1134/S0030400X13080092.

[14] R. Gaebel, N. Ma, J. Liu, J. Guan, L. Koch, C. Klopsch, M. Gruene, A. Toelk, W. Wang, P. Mark, F. Wang, B. Chichkov, W. Li, G. Steinhoff, Patterning human stem cells and endothelial cells with laser printing for cardiac regeneration, Biomaterials 32 (2011) 9218–9230, https://doi.org/10.1016/j.biomaterials.2011.08.071.

[15] J. Zhang, W. Xia, P. Liu, Q. Cheng, T. Tahi, W. Gu, B. Li, Chitosan modification and pharmaceutical/biomedical applications, Mar. Drugs 8 (2010) 1962–1987, https://doi.org/10.3390/md8071962.

[16] Y. Liu, S Wang, R. Zhang, Composite poly(lactic acid)/chitosan nanofibrous scaffolds for cardiac tissue engineering, Int. J. Biol. Macromol. 103 (2017) 1130–1137, https://doi.org/10.1016/j.ijbiomac.2017.05.101.

[17] P. Benzoni, P. Ginestra, L. Altomare, A. Fiorentino, L. De Nardo, E. Ceretti, P. Dell'Era, Biomanufacturing of a chitosan/collagen scaffold to drive adhesion and alignment of human cardiomyocyte derived from stem cells, Procedia CIRP 49 (2016) 113–120, https://doi.org/10.1016/j.procir.2015.09.004.

[18] P. Baei, S. Jalili-Firoozinezhad, S. Rajabi-Zeleti, M. Tafazzoli-Shadpour, H. Baharvand, N. Aghdami, Electrically conductive gold nanoparticle-chitosan thermosensitive hydrogels for cardiac tissue engineering, Mater. Sci. Eng. C 63 (2016) 131–141, https://doi.org/10.1016/j.msec.2016.02.056.

[19] L.A. Reis, L.L.Y. Chiu, Y. Liang, K. Hyunh, A. Momen, M. Radisic, A peptide-modified chitosan–collagen hydrogel for cardiac cell culture and delivery, Acta Biomater. 8 (2012) 1022–1036, https://doi.org/10.1016/j.actbio.2011.11.030.

[20] M.D. Dozois, L.C. Bahlmann, Y. Zilberman, X. (Shirley) Tang, Carbon nanomaterial-enhanced scaffolds for the creation of cardiac tissue constructs: a new frontier in cardiac tissue engineering, Carbon N. Y. 120 (2017) 338–349, https://doi.org/10.1016/j.carbon.2017.05.050.

[21] B. Sitharaman, X. Shi, X.F. Walboomers, H. Liao, V. Cuijpers, L.J. Wilson, A.G. Mikos, J.A. Jansen, In vivo biocompatibility of ultra-short single-walled carbon nanotube/biodegradable polymer nanocomposites for bone tissue engineering, Bone 43 (2008) 362–370, https://doi.org/10.1016/j.bone.2008.04.013.

[22] D. Dean, J. Wallace, A. Siblani, M.O. Wang, K. Kim, A.G. Mikos, J.P. Fisher, Continuous digital light processing (cDLP): highly accurate additive manufacturing of tissue engineered bone scaffolds, Virtual Phys. Prototyp. 7 (2012) 13–24, https://doi.org/10.1080/17452759.2012.673152.

[23] H. Ikehata, T. Ono, The mechanisms of UV mutagenesis, J. Radiat. Res. 52 (2011) 115–125, https://doi.org/10.1269/jrr.10175.

[24] K.N. Bardakova, T.A. Akopova, A.V. Kurkov, G.P. Goncharuk, D.V. Butnaru, V.F. Burdukovskii, A.A. Antoshin, I.A. Farion, T.M. Zharikova, A.B. Shekhter, V.I. Yusupov, P.S. Timashev, Y.A. Rochev, From aggregates to porous three-dimensional scaffolds through a mechanochemical approach to design photosensitive chitosan derivatives, Mar. Drugs 17 (2019) 48, https://doi.org/10.3390/md17010048.

[25] A. Kroustalli, A.E. Zisimopoulou, S. Koch, L. Rongen, D. Deligianni, S. Diamantouros, G. Athanassiou, M. Kokozidou, D. Mavrilas, S. Jockenhoevel, Carbon nanotubes reinforced chitosan films: mechanical properties and cell response of a novel biomaterial for cardiovascular tissue engineering, J. Mater. Sci. Mater. Med. 24 (2013) 2889–2896, https://doi.org/10.1007/s10856-013-5029-8.

[26] A.V. Ilyina, V.E. Tikhonov, A.I. Albulov, V.P. Varlamov, Enzymic preparation of acid-free-water-soluble chitosan, Process Biochem. 35 (2000) 563–568, https://doi.org/10.1016/S0032-9592(99)00104-1.

[27] P. Kumbhakar, A.K. Kole, C.S. Tiwary, S. Biswas, S. Vinod, J. Taha-Tijerina, U. Chatterjee, P.M. Ajayan, Nonlinear optical properties and temperature-dependent UV-vis absorption and photoluminescence emission in 2D hexagonal boron nitride nanosheets, Adv. Opt. Mater. 3 (2015) 828–835, https://doi.org/10.1002/adom.201400445.

[28] R.Y. Krivenkov, T.N. Mogileva, K.G. Mikheev, A.V. Okotrub, G.M. Mikheev, Heat-induced dip of optical limiting threshold in carbon nanotube Aqueous suspension, J. Phys. Chem. C 122 (2018) 16339–16345, https://doi.org/10.1021/acs.jpcc.8b02413.

[29] S.A. Tereshchenko, V.M. Podgaetskii, A.Y. Gerasimenko, M.S. Savel'ev, Investigation of nonlinear characteristics of intensity limiters of high-power laser radiation, Optic Spectrosc. 116 (2014) 454–461, https://doi.org/10.1134/S0030400X14030217.

[30] H. Staroszczyk, K. Sztuka, J. Wolska, A. Wojtasz-Pająk, I. Kołodziejska, Interactions of fish gelatin and chitosan in uncrosslinked and crosslinked with EDC films: FT-IR study, Spectrochim. Acta Part A Mol. Biomol. Spectrosc. 117 (2014) 707–712, https://doi.org/10.1016/j.saa.2013.09.044.

[31] S.Y. Chae, M.-K. Jang, J.-W. Nah, Influence of molecular weight on oral absorption of water soluble chitosans, J. Contr. Release 102 (2005) 383–394, https://doi.org/10.1016/j.jconrel.2004.10.012.

[32] M.N.V.R. Kumar, R.A.A. Muzzarelli, C. Muzzarelli, H. Sashiwa, A.J. Domb, Chitosan chemistry and pharmaceutical perspectives, Chem. Rev. 104 (2004) 6017–6084, https://doi.org/10.1021/cr030441b.

[33] R. Graupner, Raman spectroscopy of covalently functionalized single-wall carbon nanotubes, J. Raman Spectrosc. 38 (2007) 673–683, https://doi.org/10.1002/jrs.1694.

[34] A.Y. Tolbin, M.S. Savelyev, A.Y. Gerasimenko, L.G. Tomilova, High-performance optical limiters based on stable phthalocyanine J-type dimers, Chem. Phys. Lett. 661 (2016) 269–273, https://doi.org/10.1016/j.cplett.2016.06.051.

[35] M.S. Savelyev, A.Y. Gerasimenko, V.M. Podgaetskii, S.A. Tereshchenko, S.V. Selishchev, A.Y. Tolbin, Conjugates of thermally stable phthalocyanine J-type dimers with single-walled carbon nanotubes for enhanced optical limiting applications, Optic Laser. Technol. 117 (2019) 272–279, https://doi.org/10.1016/j.optlastec.2019.04.036.

[36] M.S. Dresselhaus, G. Dresselhaus, A. Jorio, A.G. Souza Filho, R. Saito, Raman spectroscopy on isolated single wall carbon nanotubes, Carbon N. Y. 40 (2002) 2043–2061, https://doi.org/10.1016/S0008-6223(02)00066-0.

[37] A. Hartschuh, H.N. Pedrosa, L. Novotny, T.D. Krauss, Simultaneous fluorescence and Raman scattering from single carbon nanotubes, Science (80-.) 301 (2003) 1354–1356, https://doi.org/10.1126/science.1087118.

[38] P.W. Barone, S. Baik, D.A. Heller, M.S. Strano, Near-infrared optical sensors based on single-walled carbon nanotubes, Nat. Mater. 4 (2004) 86–92, https://doi.org/10.1038/nmat1276.

[39] T. Kampfrath, K. von Volkmann, C.M. Aguirre, P. Desjardins, R. Martel, M. Krenz, C. Frischkorn, M. Wolf, L. Perfetti, Mechanism of the far-infrared absorption of carbon-nanotube films, Phys. Rev. Lett. 101 (2008) 267403, https://doi.org/10.1103/PhysRevLett.101.267403.

[40] R. Krupke, F. Hennrich, O. Hampe, M.M. Kappes, Near-infrared absorbance of single-walled carbon nanotubes dispersed in dimethylformamide, J. Phys. Chem. B 107 (2003) 5667–5669, https://doi.org/10.1021/jp034077w.

[41] A. Sionkowska, B. Kaczmarek, K. Lewandowska, S. Grabska, M. Pokrywczyńska, T. Kloskowski, T. Drewa, 3D composites based on the blends of chitosan and collagen with the addition of hyaluronic acid, Int. J. Biol. Macromol. 89 (2016) 442–448, https://doi.org/10.1016/j.ijbiomac.2016.04.085.

[42] A. Lauto, J. Hook, M. Doran, F. Camacho, L.A. Poole-Warren, A. Avolio, L.J.R. Foster, Chitosan adhesive for laser tissue repair: in vitro characterization, Laser Surg. Med. 36 (2005) 193–201, https://doi.org/10.1002/lsm.20145.

[43] Y. Xiong, J. Si, L. Yan, H. Song, W. Yi, X. Hou, The influence of nonlinear scattering light distributions on the optical limiting properties of carbon nanotubes, Laser Phys. Lett. 11 (2014) 115904, , https://doi.org/10.1088/1612-2011/11/11/115904.

[44] A.K. Nair, A. Mayeen, L.K. Shaji, M.S. Kala, S. Thomas, N. Kalarikkal, Optical characterization of nanomaterials, Charact. Nanomater. Elsevier, 2018, pp. 269–299, , https://doi.org/10.1016/B978-0-08-101973-3.00010-9.

[45] M. Tajdidzadeh, A.B. Zakaria, Z.A. Talib, A.S. Gene, S. Shirzadi, Optical nonlinear properties of gold nanoparticles synthesized by laser ablation in polymer solution, J. Nanomater. 2017 (2017) 1–9, https://doi.org/10.1155/2017/4803843.

[46] A. Tan, S. Madani, J. Rajadas, G. Pastorin, A.M. Seifalian, Synergistic photothermal ablative effects of functionalizing carbon nanotubes with a POSS-PCU nanocomposite polymer, J. Nanobiotechnol. 10 (2012) 34, https://doi.org/10.1186/1477-3155-10-34.

[47] B. Anand, S. Addo Ntim, V. Sai Muthukumar, S. Siva Sankara Sai, R. Philip, S. Mitra, Improved optical limiting in dispersible carbon nanotubes and their metal oxide hybrids, Carbon N. Y. 49 (2011) 4767–4773, https://doi.org/10.1016/j.carbon.2011.06.086.

[48] Q. Wang, H. Tang, Q. Xie, L. Tan, Y. Zhang, B. Li, S. Yao, Room-temperature ionic liquids/multi-walled carbon nanotubes/chitosan composite electrode for electrochemical analysis of NADH, Electrochim. Acta 52 (2007) 6630–6637, https://doi.org/10.1016/j.electacta.2007.04.057.

[49] L. Lu, W. Chen, Biocompatible composite actuator: a supramolecular structure consisting of the biopolymer chitosan, carbon nanotubes, and an ionic liquid, Adv. Mater. 22 (2010) 3745–3748, https://doi.org/10.1002/adma.201001134.

[50] H. Wei, L. Han, Y. Tang, J. Ren, Z. Zhao, L. Jia, Highly flexible heparin-modified chitosan/graphene oxide hybrid hydrogel as a super bilirubin adsorbent with excellent hemocompatibility, J. Mater. Chem. B. 3 (2015) 1646–1654, https://doi.org/10.1039/C4TB01673D.